SUPPLEMENTARY INFORMATION (SI)

Potential-dependent NRR/HER competition and N_2 activation mechanism in M1M2@C_6N_6 bimetallic catalysts

Lintao Xu[1], Yuhong Huang[1,3,*], Ruhai Du[1], Haiping Lin[1,3], Han Xie[1], Baiyan Zhou[1], Fei Ma[2,3,*], Xiumei Wei[1,3]

[1] *School of Physics & Information Technology, Shaanxi Normal University, Xi'an 710119, Shaanxi, China*

[2] *State Key Laboratory for Mechanical Behavior of Materials, Xi'an Jiaotong University, Xi'an 710049, Shaanxi, China*

[3] *Shaanxi "Four Bodies and One Union" University-Enterprise Joint Research Center for Advanced Molybdenum-based Functional Materials, Xi'an 710119, Shaanxi, China*

[*]Corresponding authors. Tel.: +86 29 81530750, E-mail: huangyh@snnu.edu.cn (Y.H. Huang),
+86 29 82668610, E-mail: mafei@mail.xjtu.edu.cn (F. Ma).

Table S1 The ΔG_{*N_2}, $\Delta G_{*N_2-*N_2H}$ and $\Delta G_{*NH_2-*NH_3}$ values of 55 M1M2@C_6N_6 DACs.

M1M2	ΔG_{*N_2-end} (eV)	ΔG_{*N_2-side} (eV)	$\Delta G_{*N_2-*N_2H-en}$ (eV)	$\Delta G_{*N_2-*HN_2-si}$ (eV)	$\Delta G_{*N_2-*N_2H-si}$ (eV)	ΔG_{*NH_2-*NH} (eV)
ScSc	/	-1.00	/	-0.25	0.89	1.28
ScTi	/	-1.00	/	-0.70	0.72	1.28
ScV	-0.88	/	-0.26	/	/	0.23
ScCr	-0.05	/	0.58	/	/	0.39
ScMn	-0.39	/	0.70	/	/	0.54
ScFe	-0.72	/	0.80	/	/	0.71
ScCo	-1.14	/	0.50	/	/	0.56
ScNi	-0.82	/	0.76	/	/	0.73
ScMo	-0.45	/	0.96	/	/	0.48
ScW	/	-1.01	/	-0.50	1.18	0.81
TiTi	/	-0.83	/	-0.08	0.93	0.82
TiV	-0.47	/	-0.05	/	/	0.62
TiCr	-0.34	/	1.07	/	/	0.48
TiMn	0.09	-0.05	/	0.01	0.36	0.87
TiFe	-0.64	-0.59	0.33	0.31	0.62	1.09
TiCo	-0.21	-0.22	0.32	0.50	0.53	0.71
TiNi	-0.49	-0.11	0.90	-0.05	0.41	0.17
TiMo	0.08	/	/	/	/	/
TiW	-0.51	-0.61	0.50	-0.18	-0.01	0.86
VV	-0.06	0.35	1.32	/	/	0.35
VCr	0.00	/	1.06	/	/	0.48
VMn	/	/	/	/	/	/
VFe	-0.27	-0.18	0.31	0.53	0.62	0.44
VCo	-0.44	-0.08	0.83	0.49	0.34	0.36
VNi	-0.47	-0.13	0.58	0.52	0.48	0.31
VMo	0.39	/	/	/	/	/
VW	-0.18	-0.17	0.60	0.07	0.14	0.83
CrCr	-1.36	-1.23	0.59	0.30	0.31	0.94
CrMn	-1.17	-1.08	0.66	0.45	0.95	0.88
CrFe	-0.30	-0.17	0.57	0.02	0.54	0.62
CrCo	-0.68	-0.53	0.68	0.68	0.91	0.91
CrNi	-0.16	/	0.59	/	/	0.64
CrMo	0.35	/	/	/	/	/
CrW	-0.31	0.10	0.06	/	/	0.86
MnMn	-0.85	-0.62	0.51	0.54	0.87	0.84

MnFe	-0.72	0.04	0.65	/	/	0.80
MnCo	-0.53	-0.27	0.73	0.91	0.86	0.48
MnNi	0.06	/	/	/	/	/
MnMo	0.07	/	/	/	/	/
MnW	-0.10	/	1.09	/	/	1.30
FeFe	-0.46	/	0.49	/	/	0.57
FeCo	-0.30	-0.00	0.31	0.73	0.75	0.71
FeNi	-0.21	0.36	0.75	/	/	0.89
FeMo	-0.15	/	1.15	/	/	0.62
FeW	-0.57	0.01	0.53	/	/	0.44
CoCo	-0.76	-0.51	0.68	1.04	1.05	0.87
CoNi	-0.29	0.13	0.89	/	/	0.37
CoMo	-0.32	-0.02	1.22	0.04	0.12	-0.12
CoW	-0.72	-0.19	0.94	0.24	0.38	0.49
NiNi	0.42	/	/	/	/	/
NiMo	-0.94	-0.14	0.84	0.21	0.10	0.04
NiW	-1.12	-0.38	0.55	0.16	0.38	0.48
MoMo	0.73	0.69	/	/	/	/
MoW	-0.05	/	-0.18	/	/	0.58
WW	-0.48	-0.30	0.49	0.04	0.02	0.31

Table S2 Fitted parameters of the potential-dependent free energy (with the form $E = aU^2 + bU + c$ and $E = -\frac{1}{2}C(U-U_{PZC})^2 + E_{PZC}$, respectively.) for M1M2@C_6N_6. U_{PZC} (V/SHE) and C (e/V) are the potential of zero charge (PZC) and capacitance of the corresponding system, respectively, and E_{PZC} (eV) is the energy of the system at the PZC.

Species	a	b	c	C	U_{PZC}	E_{PZC}
ScV	-1.16	-1.61	-428.13	2.31	-0.70	-427.57
*N_2-ScV	-1.19	-1.99	-446.00	2.39	-0.83	-445.17
*H-ScV	-1.08	-1.30	-432.51	2.16	-0.60	-432.12
ScMn	-1.11	-0.05	-427.43	2.22	-0.02	-427.43
*N_2-ScMn	-1.14	-0.48	-445.95	2.29	-0.21	-445.90
*H-ScMn	-0.92	-0.07	-431.26	1.83	-0.04	-431.25

*N_2H-ScMn	-1.06	-0.46	-448.96	2.11	-0.21	-448.91
*N_2H_2-ScMn	-1.14	-0.94	-452.75	2.29	-0.41	-452.56
*N-ScMn	-1.03	-0.31	-436.80	2.07	-0.15	-436.78
*NH-ScMn	-1.12	-0.60	-440.95	2.23	-0.27	-440.87
*NH_2-ScMn	-1.14	-0.79	-445.34	2.28	-0.35	-445.20
*NH_3-ScMn	-1.10	-1.11	-449.06	2.20	-0.50	-448.78
ScCo	-1.14	-0.41	-425.50	2.29	-0.18	-425.46
*N_2-ScCo	-1.11	-0.45	-444.13	2.22	-0.20	-444.08
*H-ScCo	-1.17	-0.45	-430.47	2.34	-0.19	-430.43
VFe	-1.17	-0.19	-427.57	2.35	-0.08	-427.56
*N_2-VFe	-1.14	0.04	-444.69	2.27	0.02	-444.68
*H-VFe	-1.14	0.07	-431.01	2.27	0.03	-431.01
*N_2H-VFe	-1.14	0.00	-448.00	2.28	0.00	-448.00
*N_2H_2-VFe	-1.05	-0.35	-451.90	2.10	-0.17	-451.87
*N-VFe	-1.10	0.03	-436.16	2.21	0.01	-436.16
*NH-VFe	-1.10	-0.22	-440.25	2.21	-0.10	-440.24
*NH_2-VFe	-1.11	-0.30	-444.47	2.22	-0.14	-444.45
*NH_3-VFe	-1.06	-0.64	-447.96	2.13	-0.30	-447.86
VNi	-1.38	-2.67	-425.57	2.76	-0.97	-424.28
*N_2-VNi	-1.07	-2.35	-443.09	2.14	-1.10	-441.81
*H-VNi	-1.06	-1.97	-429.35	2.12	-0.93	-428.44
FeW	-1.03	-2.27	-430.67	2.06	-1.10	-429.42

*N_2-FeW	-1.05	-2.28	-448.39	2.09	-1.09	-447.14
*H-FeW	-0.95	-1.82	-434.49	1.89	-0.96	-433.62
NiW	-1.04	-2.39	-427.52	2.08	-1.15	-426.14
*N_2-NiW	-0.92	-1.98	-445.22	1.85	-1.07	-444.16
*H-NiW	-0.88	-1.57	-431.24	1.76	-0.89	-430.54
WW	-1.44	-2.75	-434.80	2.88	-0.95	-433.49
*N_2-WW	-1.26	-2.45	-452.61	2.52	-0.98	-451.41
*H-WW	-1.03	-1.97	-438.83	2.06	-0.96	-437.89

Table S3 The feature names and their corresponding symbols of the original feature set.

feature	symbol
The interatomic distance between M1 and M2	d_{M1M2}
The atomic number of M1	Z_{M1}
The atomic radius of M1	R_{M1}
The first ionization energy of M1	I_{M1}
The pauling electronegativity of M1	χ_{M1}
Unpaired d-electron number of M1	$N_{ied,M1}$
The covalent radius of M1	$R_{COV,M1}$
The number of outermost d electrons of M1	$N_{d,M1}$
The electron affinity of M1	$E_{A,M1}$
The relative atomic mass of M1	M_{M1}
The oxide formation enthalpy of M1	$H_{f,oxM1}$
Average distance between M1 and the coordinating N atoms	d_{M1-N}
The atomic number of M2	Z_{M2}
The atomic radius of M2	R_{M2}
The first ionization energy of M2	I_{M2}
The pauling electronegativity of M2	χ_{M2}

Unpaired d-electron number of M2	$N_{ied,M2}$
The covalent radius of M2	$R_{COV,M2}$
The number of outermost d electrons of M2	$N_{d,M2}$
The electron affinity of M2	$E_{A,M2}$
The relative atomic mass of M2	M_{M2}
The oxide formation enthalpy of M2	$H_{f,oxM2}$
Average distance between M2 and the coordinating N atoms	d_{M2-N}
$\chi_{M1} + \chi_{M2}$	χ_{M+}
$\chi_{M1} - \chi_{M2}$	χ_{M-}
$N_{ied,M1} + N_{ied,M2}$	$N_{ied,+}$
$N_{ied,M1} - N_{ied,M2}$	$N_{ied,-}$
$N_{d,M1} + N_{d,M2}$	$N_{d,+}$
$N_{d,M1} - N_{d,M2}$	$N_{d,-}$

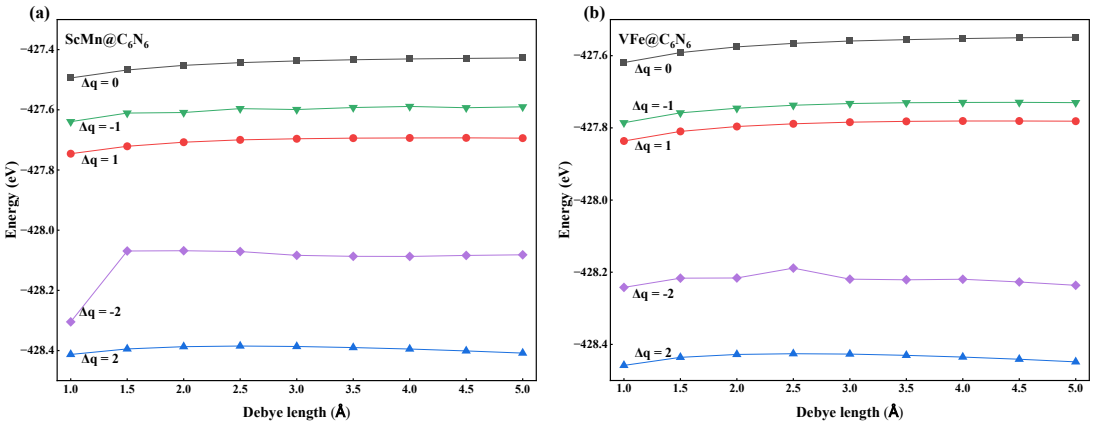

Fig. S1 Convergence test of the Debye length

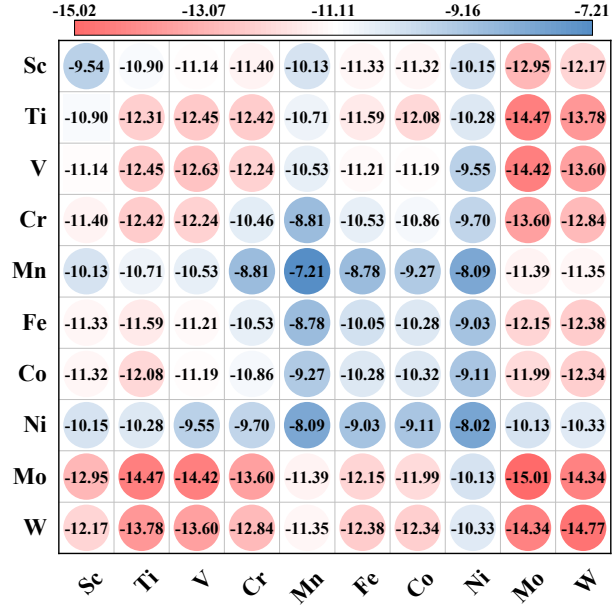

Fig. S2 The heatmap of E_{bin} of M1M2@C_6N_6. the Gibbs free energy change of N_2 adsorption through end-on and side-on configurations on (b) TM@N_4, (c) TM@S_1N_3, (d) TM@$S_2N_{2\text{-PEN}}$, (e) TM@$S_2N_{2\text{-HEX}}$, (f) TM@$S_2N_{2\text{-OPP}}$, (g) TM@S_3N_1 and (h) TM@S_4, respectively.

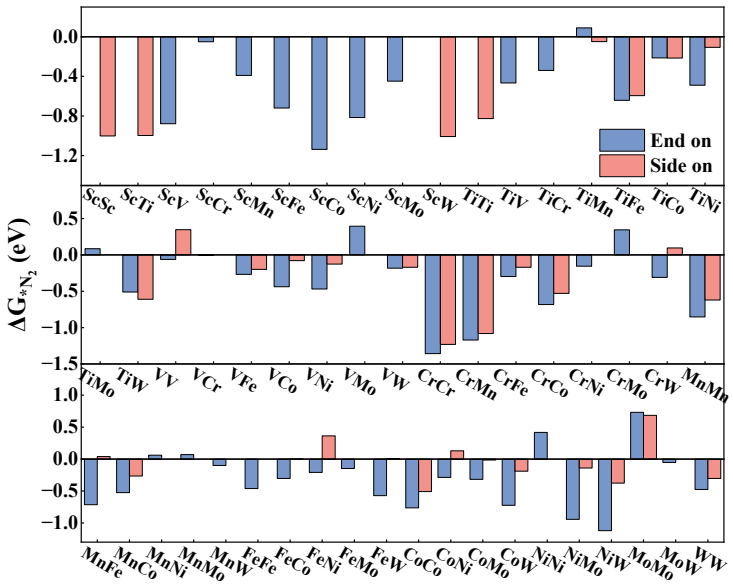

Fig. S3 The Gibbs free energy change of N_2 adsorption through end-on and side-on configurations on M1M2@C_6N_6.

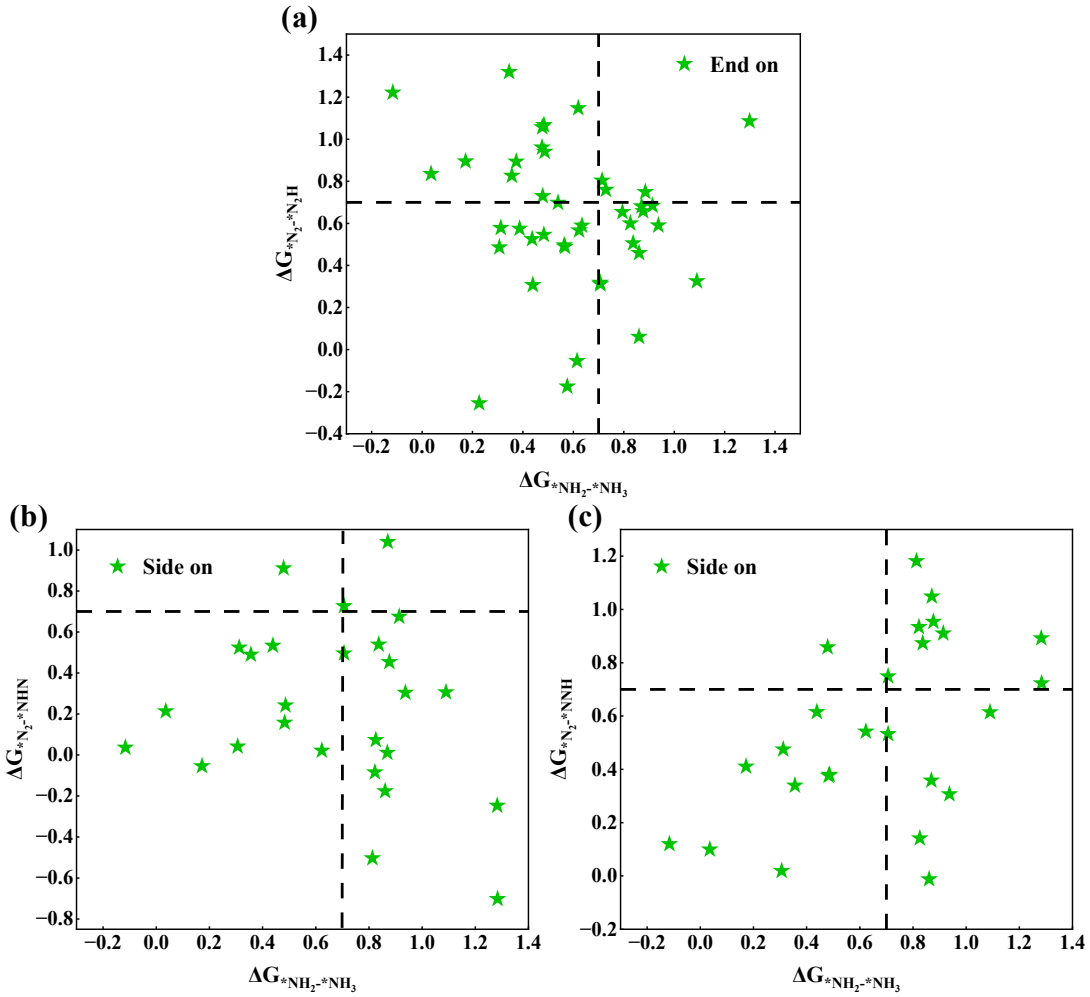

Fig. S4 The Gibbs free energy for the first and last hydrogenation steps of M1M2@C_6N_6.

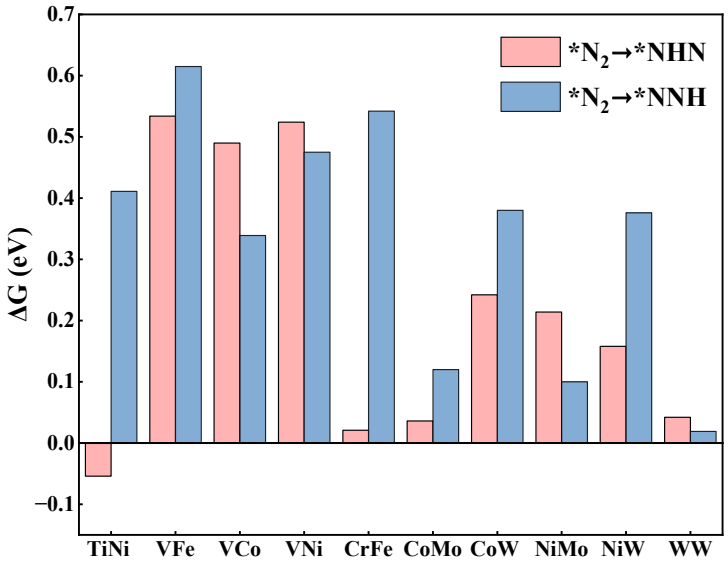

Fig. S5 Comparison of hydrogenation free energies for 9 candidate catalysts meeting the screening criteria in side-on mode.

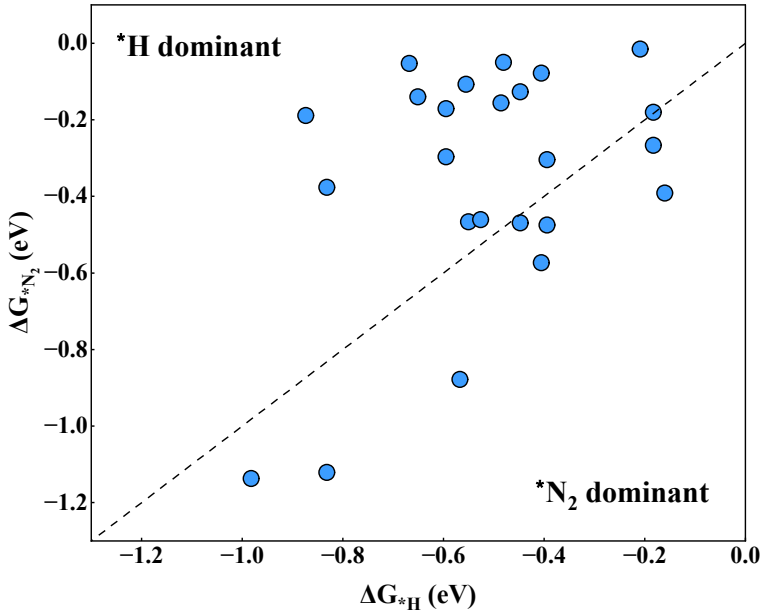

Fig. S6 The competition of HER and NRR by comparing ΔG_{*H} and ΔG_{*N_2} to evaluate catalytic selectivity.

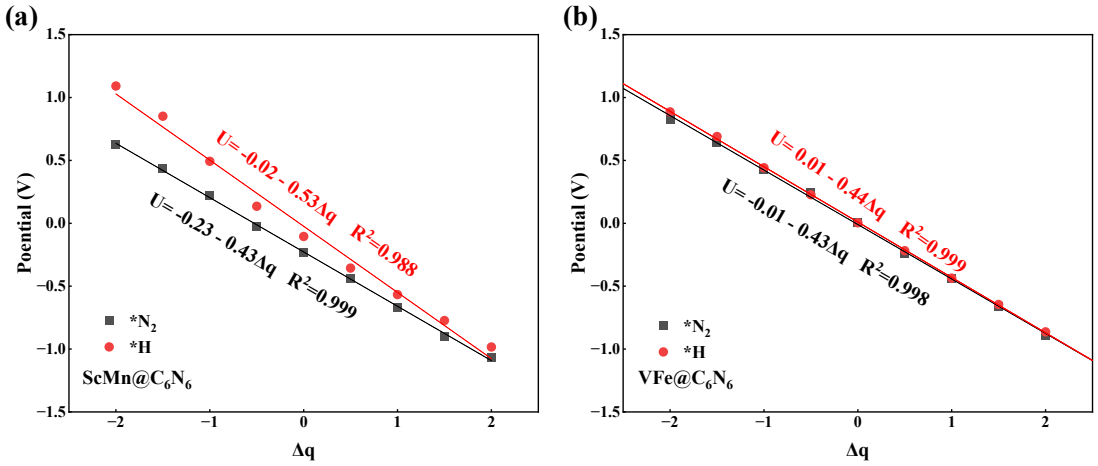

Fig. S7 Relationship between applied potential and extra electrons for ScMn@C_6N_6 and VFe@C_6N_6.

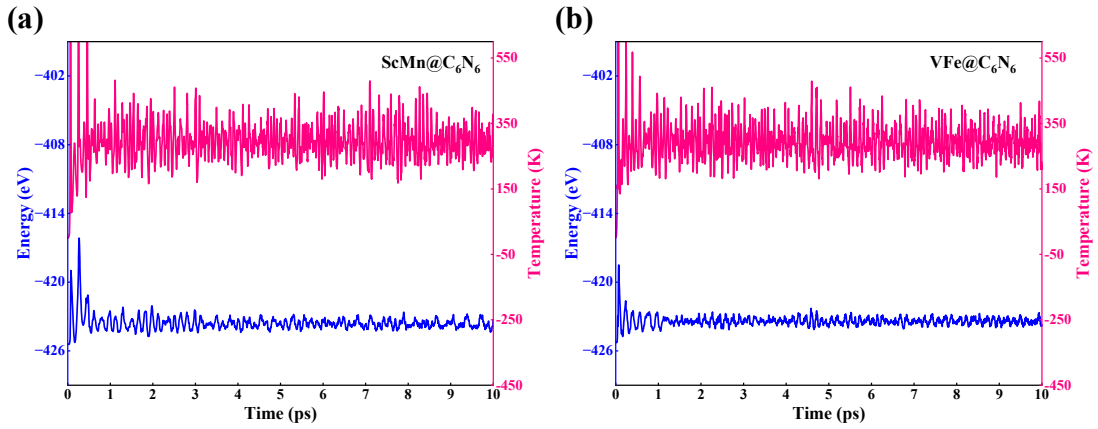

Fig. S8 The variations of temperature and energy change with elapsed time of 10 ps at 300 K of (a) ScMn@C_6N_6 and (b) VFe@C_6N_6 during the AIMD simulation, respectively.

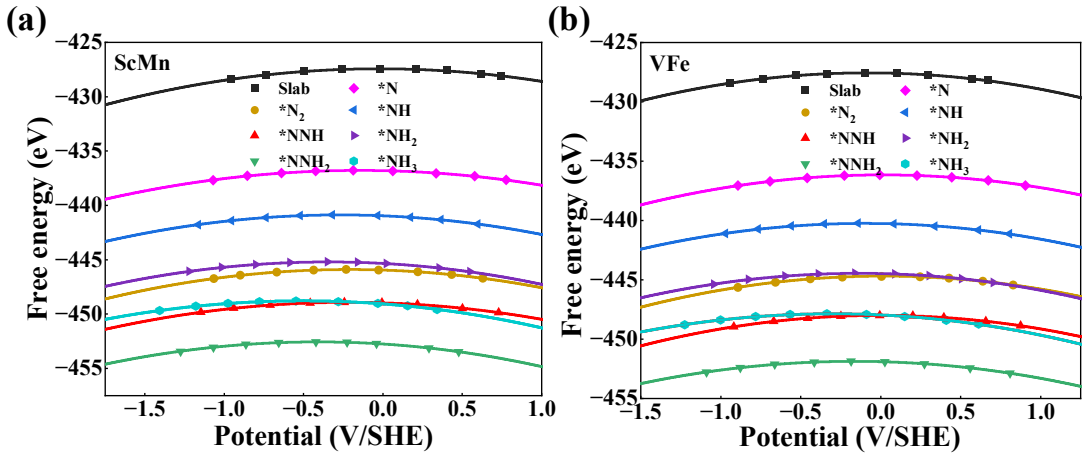

Fig. S9 Calculated energies of the bare (a) ScMn, (b) VFe@C_6N_6 and seven reaction intermediates as a function of different electrode potentials.

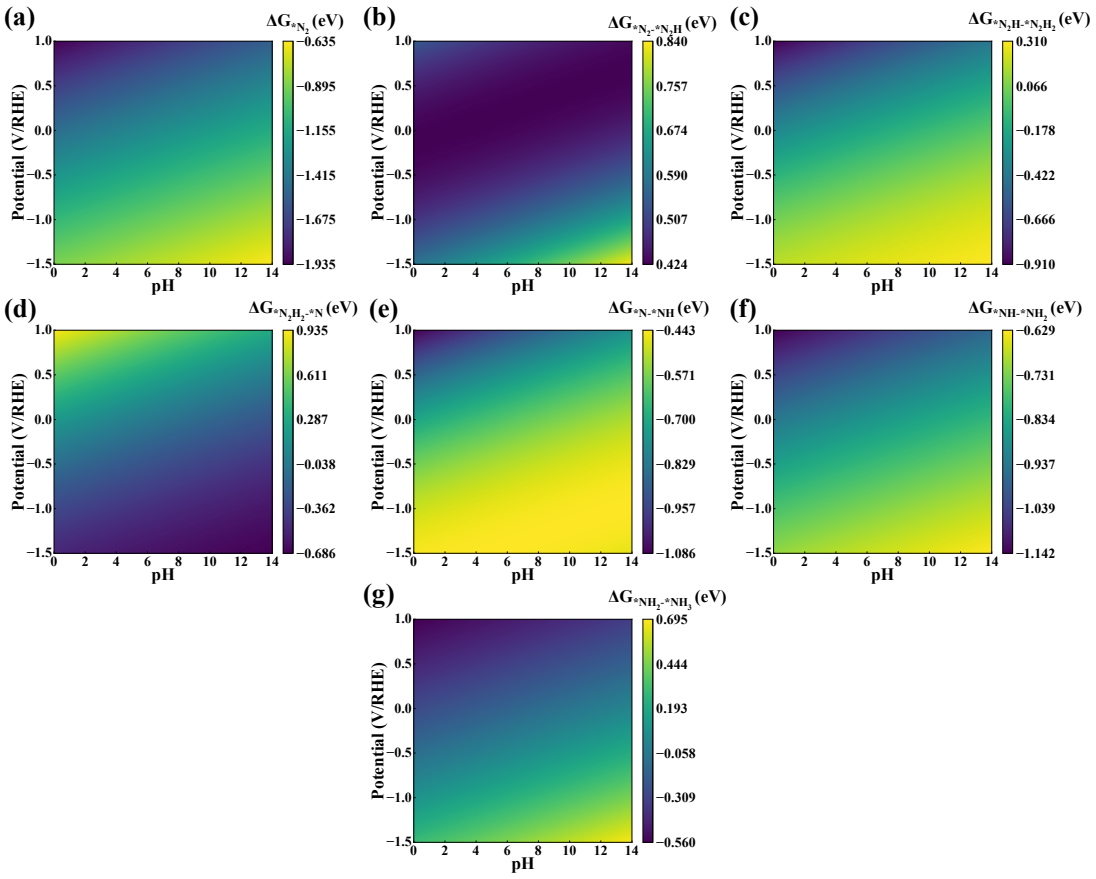

Fig. S10 Contour maps of the reaction free energies for ScMn@C_6N_6 as a function of pH values and applied potentials.

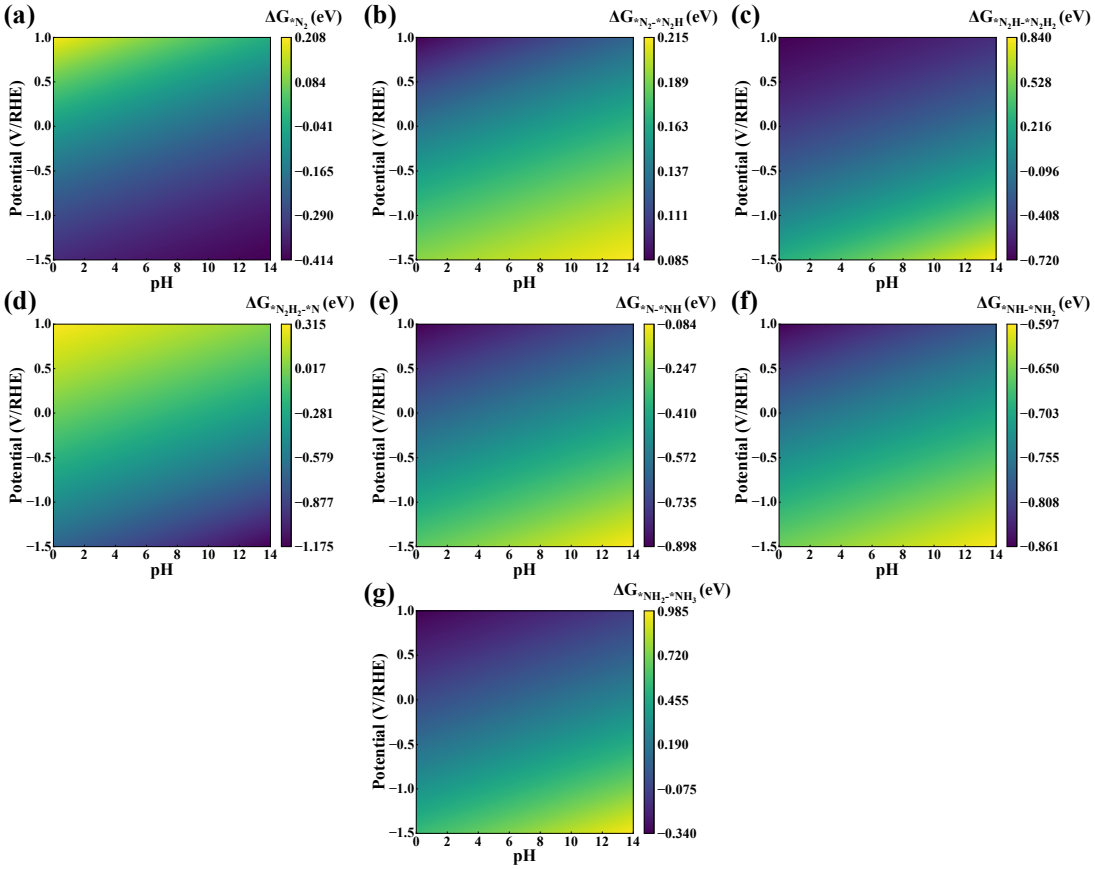

Fig. S11 Contour maps of the reaction free energies for VFe@C_6N_6 as a function of pH values and applied potentials.

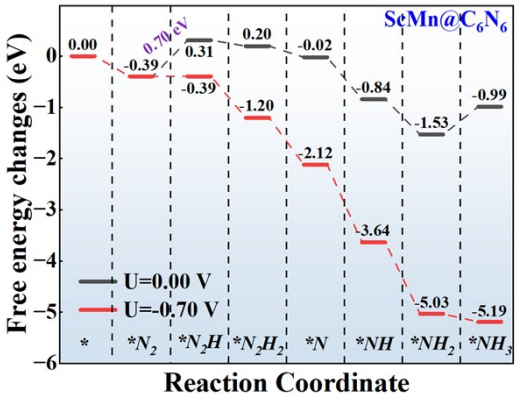

Fig. S12 Gibbs free energy change diagram of ScMn@C_6N_6 along the distal pathway under vacuum conditions.

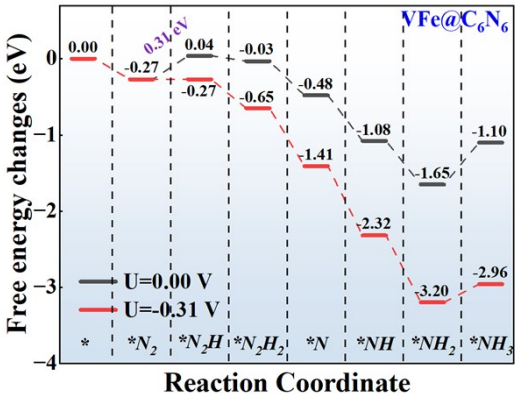

Fig. S13 Gibbs free energy change diagram of $VFe@C_6N_6$ along the distal pathway under vacuum conditions.

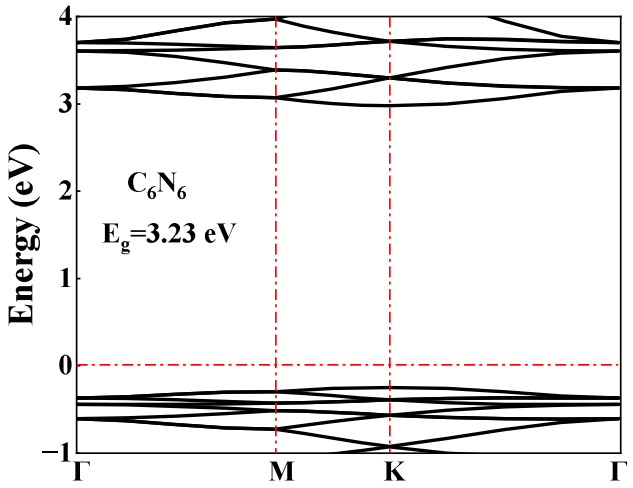

Fig. S14 The electronic band structure of C_6N_6.

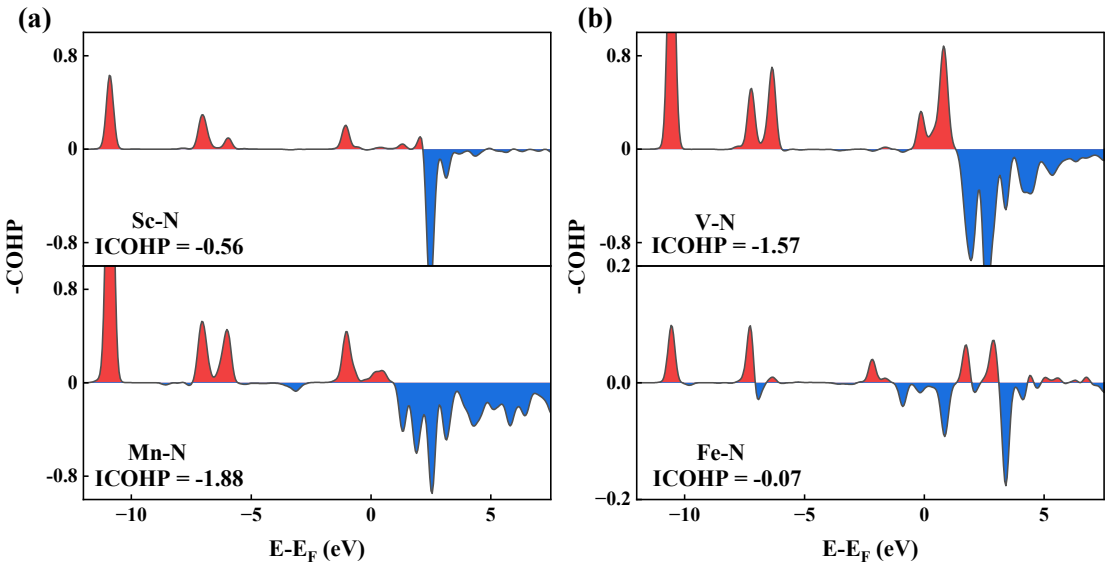

Fig. S15 The COHP of (a) $ScMn@C_6N_6$ and (b) $VFe@C_6N_6$.

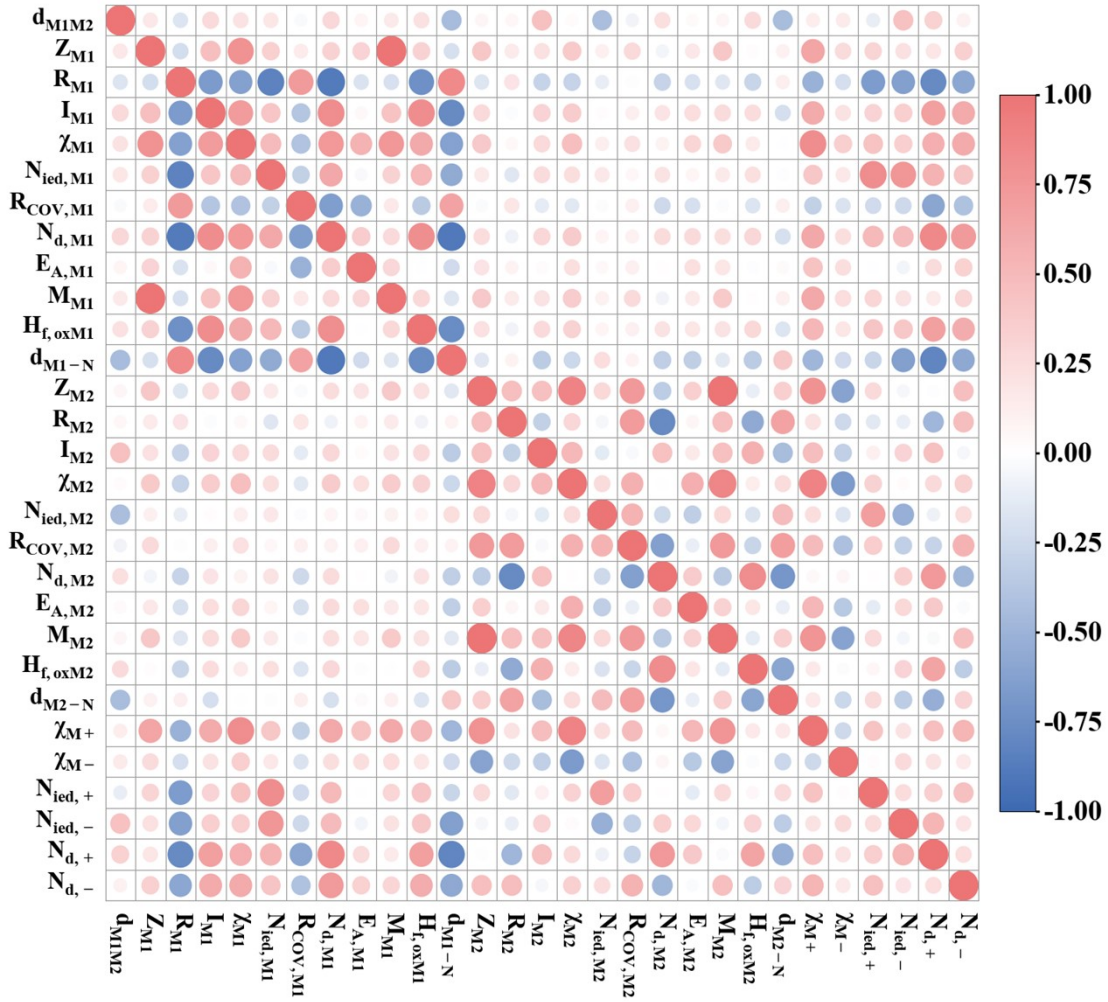

Fig. S16 Pearson correlation plots of raw feature set.

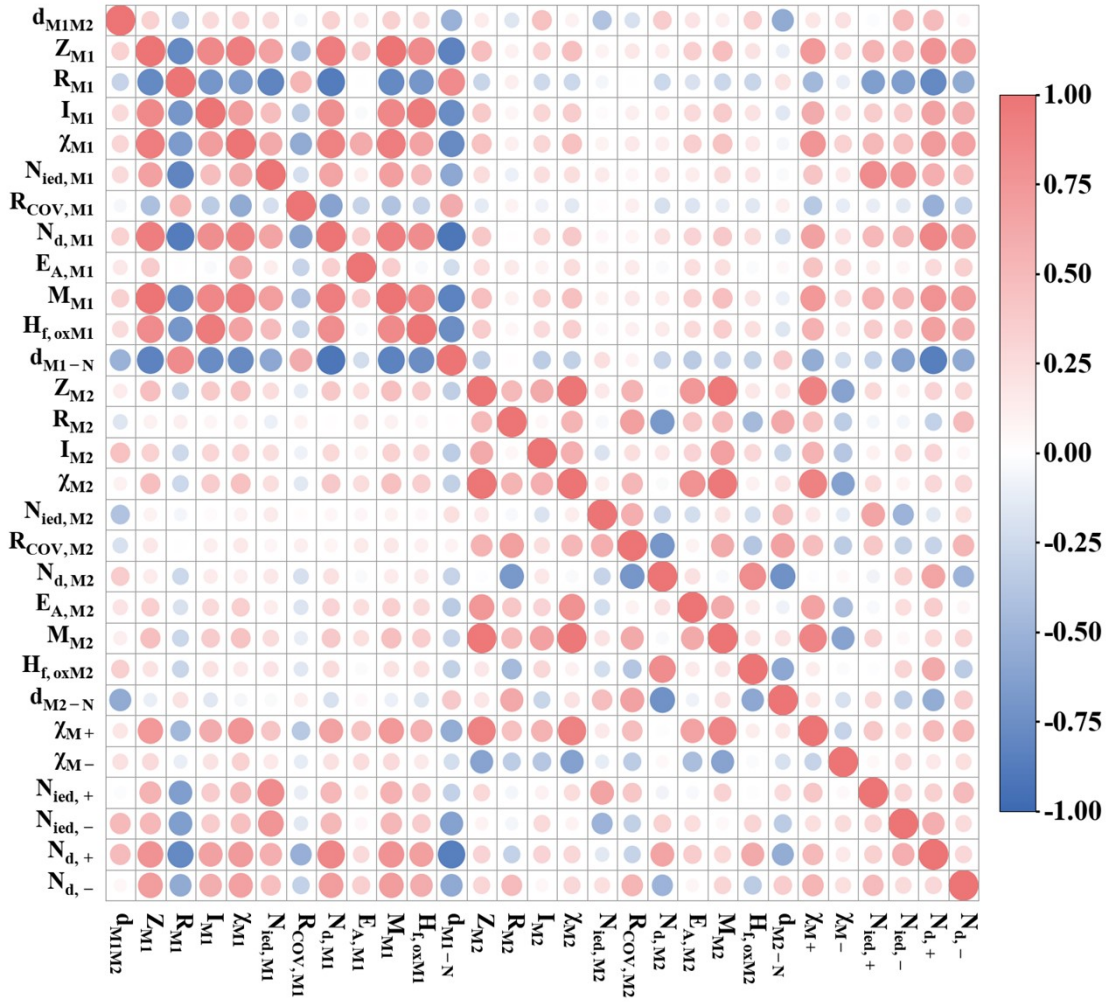

Fig. S17 Spearman correlation plots of raw feature set.

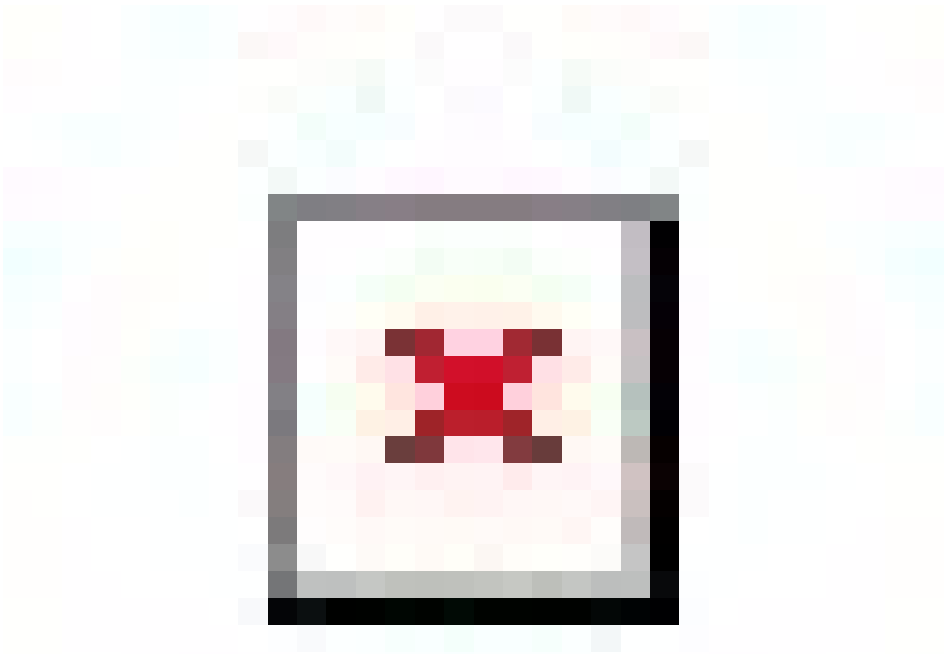

Fig. S18 Pearson correlation plots of refined feature set.

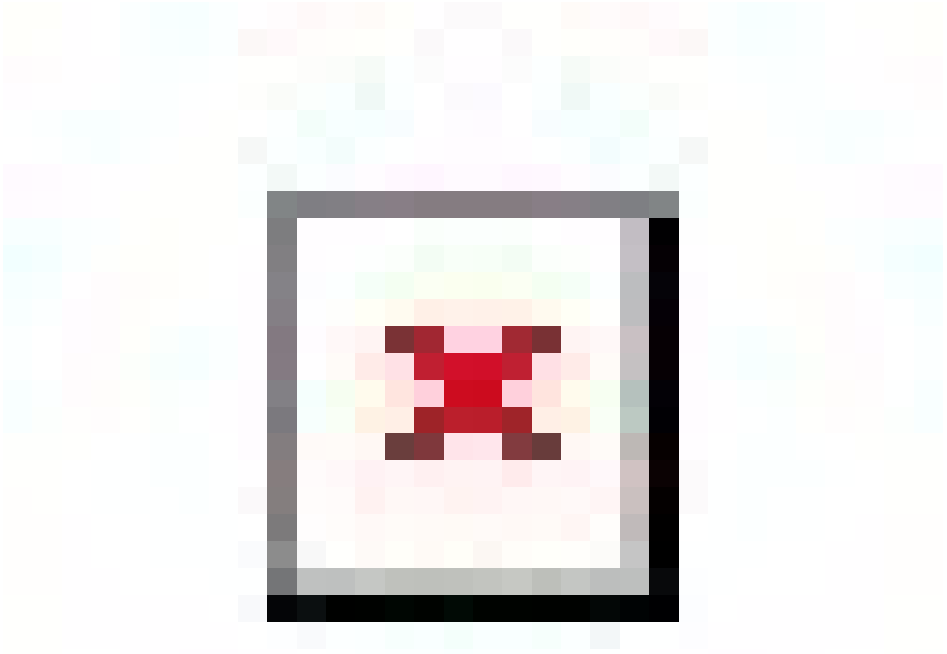

Fig. S19 Spearman correlation plots of refined feature set.

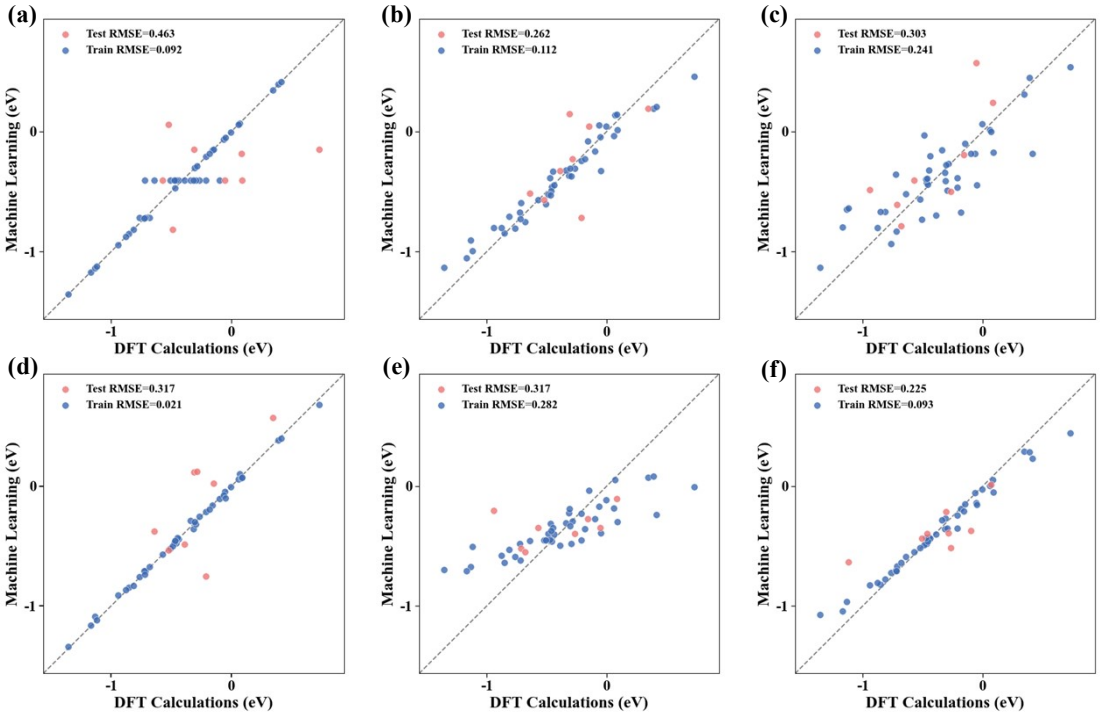

Fig. S20 Comparison of the adsorption free energies of ΔG_{*N_2-end} obtained by DFT and (a) DT, (b) LGBM, (c) RID, (d) MLP, (e) RF, (f) XGB model.

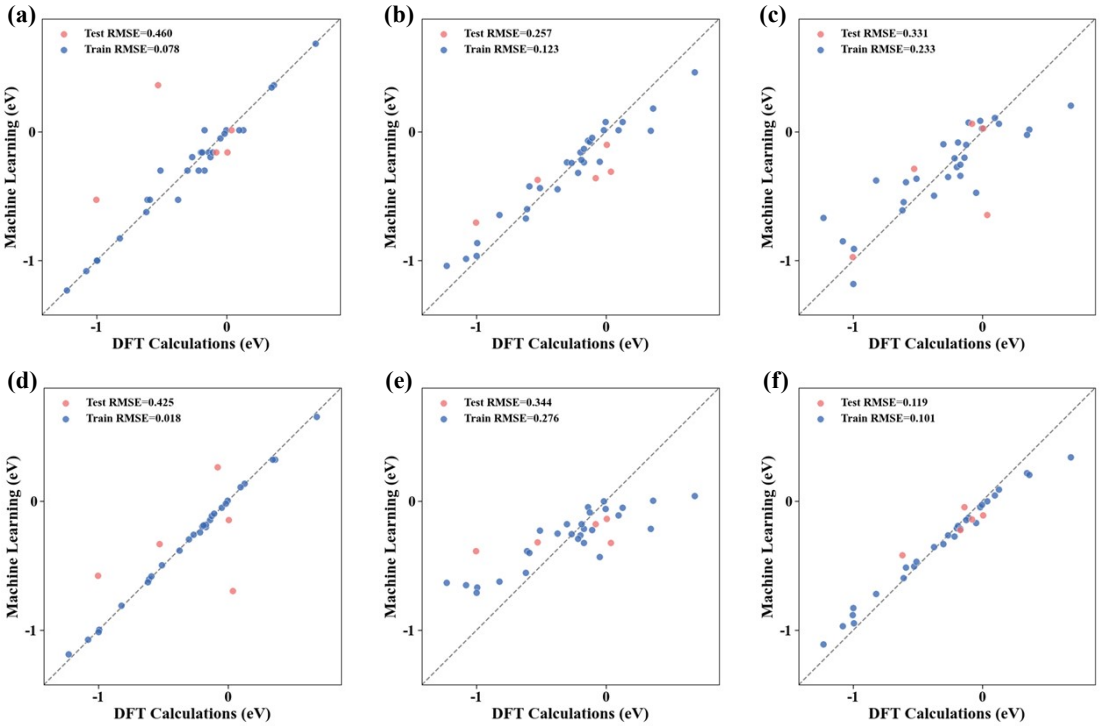

Fig. S21 Comparison of the adsorption free energies of ΔG_{*N_2-side} obtained by DFT and (a) DT, (b) LGBM, (c) RID, (d) MLP, (e) RF, (f) XGB model.

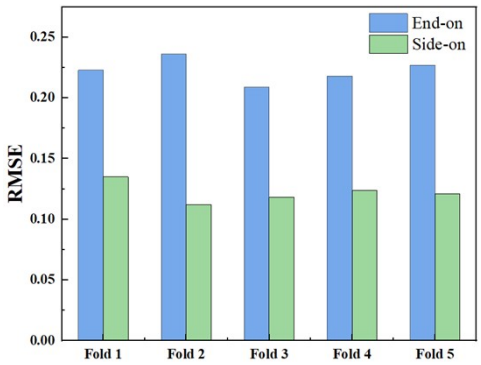

Fig. S22 The assessment of generalization capability of the XGB model under 5-fold cross validation.